Check for updates

AGU ADVANCING EARTH AND SPACE SCIENCES

Earth and Space Science

RESEARCH ARTICLE
10.1029/2023EA003482

Evaluation of PRISMA Products Over Snow in the Alps and Antarctica

B. Di Mauro[1], S. Cogliati[2], N. Bohn[3], G. Traversa[1], R. Garzonio[2], G. Tagliabue[2], G. Bramati[2,4], E. Cremonese[5], T. Julitta[6], L. Guanter[7], A. Kokhanovsky[8], C. Giardino[9], C. Panigada[2], M. Rossini[2], and R. Colombo[2]

[1]Institute of Polar Sciences, National Research Council, Milan, Italy, [2]Department of Earth and Environmental Sciences, University of Milano-Bicocca, Milan, Italy, [3]Jet Propulsion Laboratory, California Institute of Technology, Pasadena, CA, USA, [4]Remote Sensing Laboratories, University of Zurich, Zürich, Switzerland, [5]CIMA Research Foundation, Savona, Italy, [6]JB Hyperspectral Devices, Dusseldorf, Germany, [7]Research Institute of Water and Environmental Engineering (IIAMA), Universitat Politècnica de València (UPV), Valencia, Spain, [8]GFZ German Research Centre for Geosciences, Potsdam, Germany, [9]Institute for Electromagnetic Sensing of the Environment, National Research Council, Milan, Italy

Abstract PRISMA is a hyperspectral satellite mission launched by the Italian Space Agency (ASI) in April 2019. The mission is designed to collect data at global scale for a variety of applications, including those related to the cryosphere. This study presents an evaluation of PRISMA Level 1 (L1) and Level 2 (L2D) products for different snow conditions. To the aim, PRISMA data were collected at three sites: two in the Western European Alps (Torgnon and Plateau Rosa) and one in East Antarctica (Nansen Ice Shelf). PRISMA data were acquired contemporary to both field measurements and Sentinel-2 data. Simulated Top of the Atmosphere (TOA) radiance data were then compared to L1 PRISMA and Sentinel-2 TOA radiance. Bottom Of Atmosphere (BOA) reflectance from PRISMA L2D and Sentinel-2 L2A data were then evaluated by direct comparison with field data. Both TOA radiance and BOA reflectance PRISMA products were generally in good agreement with field data, showing a Mean Absolute Difference (MAD) lower than 5%. L1 PRISMA TOA radiance products resulted in higher MAD for the site of Torgnon, which features the highest topographic complexity within the investigated areas. In Plateau Rosa we obtained the best comparison between PRISMA L2D reflectance data and in situ measurements, with MAD values lower than 5% for the 400–900 nm range. The Nansen Ice Shelf instead resulted in MAD values <10% between PRISMA L2D and field data, while Sentinel-2 BOA reflectance showed higher values than other data sources.

Plain Language Summary Satellite imaging spectroscopy data provide valuable information on Earth surface processes. In this study we evaluated data acquired from the PRISMA satellite mission in the Alps and Antarctica. Those studies are important to validate satellite observations with contemporary field measurements since they open the possibility of quantitatively use PRISMA data for cryosphere monitoring.

Key Points:

- We present an evaluation of PRISMA Level 1 and Level 2 products for different snow conditions
- Contemporary to PRISMA acquisition, field spectroscopy data were collected on snow in the Alps and in Antarctica
- Both radiance and reflectance PRISMA products were generally in good agreement with field data

Correspondence to:

B. Di Mauro,
biagio.dimauro@cnr.it

Citation:

Di Mauro, B., Cogliati, S., Bohn, N., Traversa, G., Garzonio, R., Tagliabue, G., et al. (2024). Evaluation of PRISMA products over snow in the Alps and Antarctica. *Earth and Space Science*, *11*, e2023EA003482. https://doi.org/10.1029/2023EA003482

Received 21 DEC 2023
Accepted 30 MAY 2024

Author Contributions:

Conceptualization: B. Di Mauro, R. Colombo
Data curation: B. Di Mauro, N. Bohn, G. Traversa, R. Garzonio, G. Tagliabue, T. Julitta
Formal analysis: S. Cogliati, N. Bohn, G. Traversa, R. Garzonio, G. Tagliabue, T. Julitta
Funding acquisition: B. Di Mauro, C. Giardino, R. Colombo
Investigation: B. Di Mauro, G. Tagliabue, G. Bramati, E. Cremonese, C. Giardino, C. Panigada
Methodology: B. Di Mauro, S. Cogliati, N. Bohn, G. Traversa, R. Garzonio, G. Tagliabue, G. Bramati, E. Cremonese, T. Julitta, L. Guanter, A. Kokhanovsky, C. Giardino, C. Panigada, M. Rossini, R. Colombo
Resources: M. Rossini, R. Colombo
Software: S. Cogliati, N. Bohn, G. Traversa, R. Garzonio, G. Tagliabue, T. Julitta

© 2024. The Author(s).
This is an open access article under the terms of the Creative Commons Attribution-NonCommercial-NoDerivs License, which permits use and distribution in any medium, provided the original work is properly cited, the use is non-commercial and no modifications or adaptations are made.

1. Introduction

Among natural surfaces, snow features unique optical properties (Kokhanovsky, 2021; Warren, 2019), reflecting most of the incoming solar radiation in the visible wavelengths and absorbing it in the short-wave infrared. The near infrared wavelengths represent a zone of transition among reflection and absorption, where the optical properties of snow are particularly influenced by the structure of the snow pack (i.e., grain shape and size distribution, liquid water content). Dry snow is characterized by high reflectance values in the visible wavelengths. As snow ages, more photons are absorbed or transmitted rather then reflected, and this induces a gradual decrease in reflectance (Dozier & Painter, 2004). The shape and magnitude of the multispectral and hyperspectral reflectance of snow has been studied in detail, mostly in relation to the possibility to estimate some relevant key properties of surface snow such as albedo, grain size, concentration and type of impurities, and liquid water content (Di Mauro et al., 2015; Green et al., 2006; Kokhanovsky et al., 2019; Painter et al., 2013). In the past, both imaging and non-imaging spectroscopy data have been efficiently used for characterizing the surface properties of snow (Bohn et al., 2021; Dumont et al., 2017; Kokhanovsky et al., 2021; Picard et al., 2016; Salzano et al., 2021). Nowadays, the use of satellite hyperspectral data could provide important spatial and temporal information regarding the state of snow and ice across the planet.

23335084, 2024, 7, Downloaded from https://agupubs.onlinelibrary.wiley.com/doi/10.1029/2023EA003482 by CochraneItalia, Wiley Online Library on [16/05/2025]. See the Terms and Conditions (https://onlinelibrary.wiley.com/terms-and-conditions) on Wiley Online Library for rules of use; OA articles are governed by the applicable Creative Commons License

Supervision: L. Guanter, A. Kokhanovsky, C. Giardino, C. Panigada, M. Rossini, R. Colombo
Validation: A. Kokhanovsky
Visualization: S. Cogliati, G. Traversa, R. Garzonio
Writing – original draft: B. Di Mauro
Writing – review & editing: B. Di Mauro, S. Cogliati, N. Bohn, G. Traversa, R. Garzonio, G. Tagliabue, G. Bramati, E. Cremonese, T. Julitta, L. Guanter, A. Kokhanovsky, C. Giardino, R. Colombo

First applications to the cryosphere from hyperspectral satellite data were based on EO-1 Hyperion data and included the mapping of glacier surficial properties (Di Mauro et al., 2017), debris mineralogy (Casey & Kääb, 2012; Casey et al., 2012) and snow properties (Negi & Kokhanovsky, 2011). In more recent years, spaceborne imaging spectroscopy missions could offer improved observations. Most notable examples are the PRISMA mission from the Italian Space Agency (ASI) (Cogliati et al., 2021), the DESIS and EnMAP missions from the German Aerospace Center (DLR) (Storch et al., 2023), as well as the Earth Surface Mineral Dust Source Investigation (EMIT) from the National Aeronautics and Space Administration (NASA) (Green et al., 2020; Thompson et al., 2024). Future global observation programs include the Copernicus Hyperspectral Imaging Mission for the Environment (CHIME) led by the European Space Agency (ESA) (Nieke & Rast, 2018) and NASA's Surface Biology and Geology (SBG) (Lee et al., 2022).

PRISMA is a satellite mission launched in April 2019. The payload consists of an imaging spectrometer operating in a push broom scanning mode and featuring 240 spectral bands ranging from 400 to 2,500 nm, with a nominal spectral sampling interval <11 nm and a bandwidth <15 nm. The 240 bands are resolved on 1,000 across-track pixels with a 12-bit radiometric resolution. PRISMA has a swath width of 30 km with a ground spatial resolution of 30 m. The system is capable of off-nadir observations which are obtained through across-track or along-track roll operations. With the launch of PRISMA, new opportunities for cryosphere monitoring were opened, as for example, for mapping glacier ice surface properties on the Greenland Ice Sheet (Bohn et al., 2022), and for deriving snow properties in Antarctica (Kokhanovsky et al., 2022).

While PRISMA products have been evaluated for cropland (Cogliati et al., 2021; Tagliabue et al., 2022), coastal and inland water (Giardino et al., 2020), non-photosyntetic vegetation (Pepe et al., 2020) and soils (Pignatti et al., 2022), no comparisons with field data are yet available for snow covered areas. Following PRISMA product evaluation studies, the objective of our work is to provide a first evaluation of PRISMA Level 1 (i.e., Top Of Atmosphere—TOA radiance) and Level 2D (i.e., Bottom Of Atmosphere—BOA reflectance) products for three experimental sites encompassing different snow conditions (dry and melting snow). Two sites are located in the European Western Alps (namely Torgnon and Plateau Rosa) and one in East Antarctica (Nansen Ice Shelf). These comparisons are necessary to validate PRISMA L1 and L2D products for snow monitoring, and to support ongoing efforts toward the validation of PRISMA mission over high reflective targets. In particular, snow reflectance in the visible and near infrared (VNIR) wavelengths is useful to evaluate data at the high radiance edge of the PRISMA dynamic range. Due to the key role the field measurements play for allowing PRISMA products to be assessed, the limitations and potential improvements for calibration/validation activities over snow are also discussed along with potential applications of PRISMA to retrieve snow parameters.

2. Materials and Methods

2.1. Study Areas and Field Campaigns

To support the PRISMA products evaluations over different snow conditions, we conducted three field campaigns synchronously with satellite overpasses. In particular, two campaigns were developed in the European Western Alps (Figure 1), both in winter and summer, and one in East Antarctica (Figure 2) during the austral summer.

The winter campaign in the Alps was organized at Torgnon (coordinates: 45°50′40″N, 7°34′41″E), a site that is part of a long term environmental monitoring program and it has been previously exploited for monitoring and modeling snow dynamics (Colombo et al., 2019; Di Mauro et al., 2019). Torgnon is an unmanaged pasture located at 2,160 m above sea level (asl), it is seasonally covered with snow typically from October to May. The site is equipped with different instruments for vegetation and snow properties monitoring.

The summer Alpine campaign was organized at the site of Plateau Rosa (coordinates: 45°56′6″N, 7°42′ 36″E) on the border between Italy and Switzerland. The site is located at 3,500 m asl, and it is part of the glacial apparatus of the Monte Rosa massif. Plateau Rosa is seasonally covered with snow during the winter season, and bare ice is occasionally exposed during warm summer seasons (e.g., summer of 2022).

The Antarctic campaign was conducted during the XXXVIII Italian expedition in Antarctica. We selected a snow covered flat area (coordinates: 74°45′20″S 163°27′26″E) on the Nansen Ice Shelf that has been recently investigated with PRISMA to retrieve optical properties of snow (Kokhanovsky et al., 2022). The site is located at 75 m asl and it is strongly impacted by katabatic wind. The area is totally flat and showed a high homogeneity of

10.1029/2023EA003482

23335084, 2024, 7, Downloaded from https://agupubs.onlinelibrary.wiley.com/doi/10.1029/2023EA003482 by CochraneItalia, Wiley Online Library on [16/05/2025]. See the Terms and Conditions (https://onlinelibrary.wiley.com/terms-and-conditions) on Wiley Online Library for rules of use; OA articles are governed by the applicable Creative Commons License

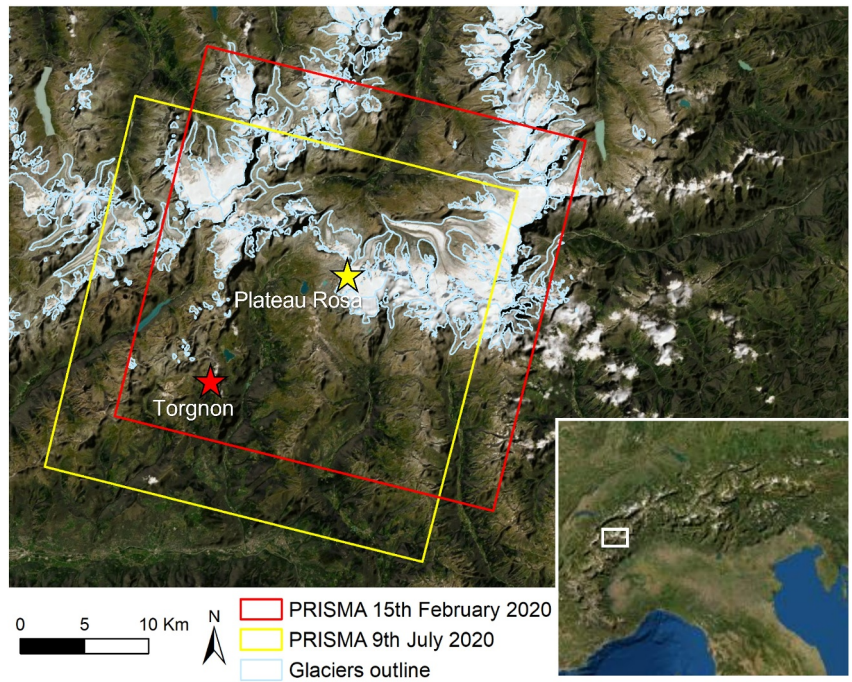

Figure 1. Location of the study areas of Torgnon and Plateau Rosa in the Western European Alps. The red rectangle refers to the footprint of the PRISMA acquisition on 15th February 2020 in Torgnon. The yellow rectangle refers to the PRISMA acquisition on 9th July 2020 in Plateau Rosa. Glaciers outline (in cyan) are taken from the latest inventory (Paul et al., 2020).

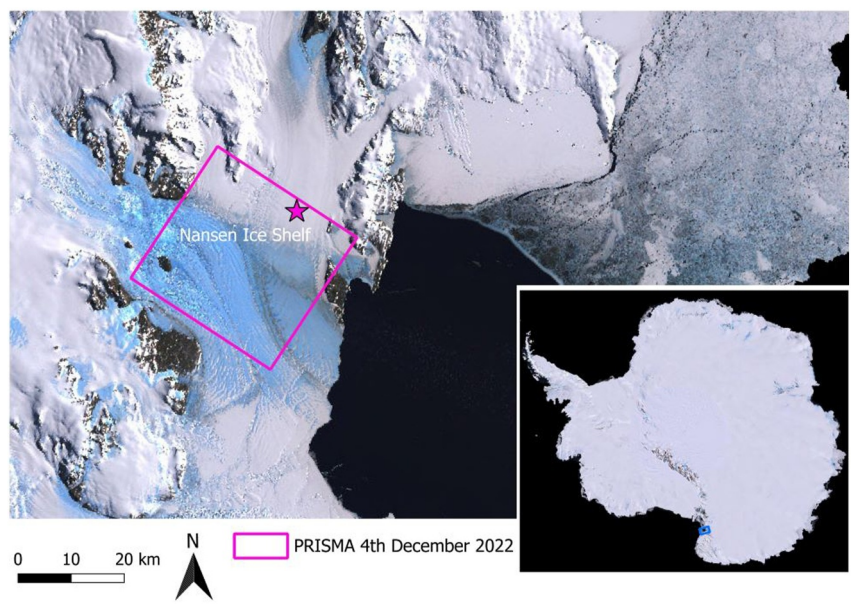

Figure 2. Location of the study area on the Nansen Ice Shelf in East Antarctica. The pink rectangle refers to the footprint of the PRISMA acquisition over the Nansen Ice Shelf (4th December 2022). The background image is taken from the LIMA mosaic of Antarctica.

23335084, 2024, 7, Downloaded from https://agupubs.onlinelibrary.wiley.com/doi/10.1029/2023EA003482 by CochraneItalia, Wiley Online Library on [16/05/2025]. See the Terms and Conditions (https://onlinelibrary.wiley.com/terms-and-conditions) on Wiley Online Library for rules of use; OA articles are governed by the applicable Creative Commons License

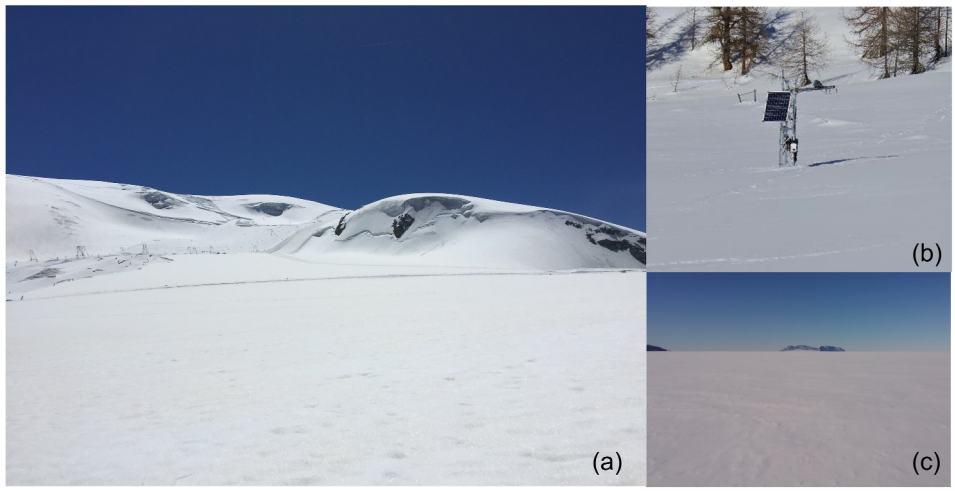

Figure 3. Experimental sites used in this study: (a) Plateau Rosa (Aosta Valley, Italy), (b) Torgnon (Aosta Valley, Italy) and (c) Nansen Ice Shelf (East Antarctica).

snow cover. In this area, dry snow is always at the ground since the air temperatures are below 0° for the whole year (Zibordi et al., 1996).

2.2. In Situ Field Spectroscopy

Field spectral measurements were collected at both Alpine sites nearly simultaneously (within ±1 hr) with respect to the PRISMA overpasses on the 15th February 2020 at Torgnon and on the 9th July 2020 at Plateau Rosa (Figure 3). The field measurements were collected using a Spectral Evolution SR-3500 spectroradiometer (Spectral Evolution, Haverhill, USA) operating from visible to shortwave infrared wavelengths (350–2,500 nm) with a spectral sampling interval of 1 nm. At the Antarctic site, we collected measurements on the 5th December 2022. In this case, we had a delay of 24 hr with respect to the PRISMA acquisition (4th December 2022). We collected measurements at the same PRISMA overpass time (±1 hr) using an Analytical Spectral Devices (ASD) Hand-held field spectrometer (Malvern Panalytical, Westborough, USA). This instrument measures the reflected radiance from 325 to 1,075 nm with a spectral sampling interval of 1 nm and a full width at half maximum (FWHM) of 3.5 nm at 700 nm. For each site, we conducted our field measurements over a rather flat area (~300 × 300 m).

For each sampling point, a set of measurements was collected a few meters apart to characterize the spectral variability of the snow-covered surface. In particular, each set included three spectral measurements over the target sandwiched between six measurements over a calibrated white reference panel (Lab-sphere, North Sutton, USA) to measure the incoming solar radiation before and after the collection of the reflected radiation of the target. The spectral measurements were collected with a Field-Of-View (FOV) of 25° at a height of 70 cm above the surface. In total, 5, 7, and 12 locations were sampled at Torgnon, Plateau Rosa and Nansen Ice Shelf, respectively. Moreover, the Torgnon site is also equipped with a fixed positioned autonomous hyperspectral radiometer (namely Reflectance box, RoX, JB Hyperpsectral Devices GmbH, Duesseldorf, Germany) that has been acquiring incident and reflected radiation every 5 min since November 2017 hence supporting also previous studies (Kokhanovsky et al., 2021). The instrument has been recently used in a global cal/val exercise for Sentinel-2 (Naethe et al., 2024). RoX raw data are converted to radiance making use of the calibration files provided by the system. Data filtering of the measurements is made using the related functionality of the GUI and based on quality flags (e.g., illumination stability during the measurement cycle, spectra saturation, and measurements collected at Solar Zenith Angle higher than 85°) based on Cogliati et al. (2015). For the final comparison, we selected the RoX measurements closer to the PRISMA satellite observation. In particular, we averaged five measurements that overlapped with the PRISMA acquisition timing.

During both Alpine field campaigns, optical properties of the atmosphere were collected with a MICROTOPS II (Solar Light Company, Inc., USA) sunphotometer at the time of PRISMA overpasses. AOT and columnar water

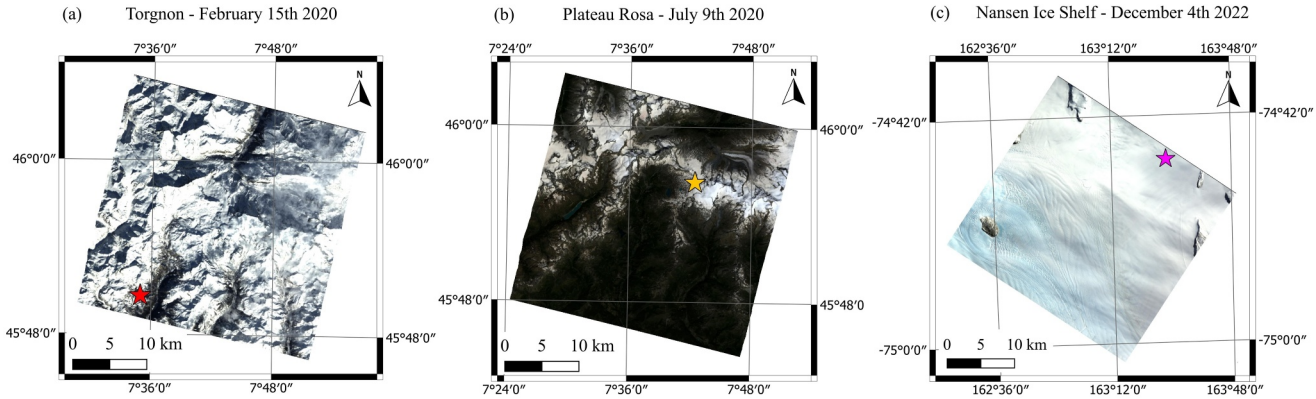

Figure 4. PRISMA L1 images (true-color composites) for Torgnon (a), Plateau Rosa (b) and Nansen Ice Shelf (c). The red, yellow and violet stars mark the field measurement sites, respectively.

vapor were retrieved from incident radiation measurements at five different wavelengths (440, 500, 870, 936, and 1020 nm). These data were used as input parameters of radiative transfer simulations of field reflectance to TOA radiance.

2.3. Satellite Data

In this study, we used hyperspectral images acquired by PRISMA and Sentinel-2 for a total of six images. Three PRISMA acquisitions were tasked contemporary to the field campaigns and successfully acquired by the sensor. Only for the Nansen Ice Shelf site, we had 1 day of delay between ground data and the satellite acquisition. The related Level 1 and Level 2D PRISMA products, storing TOA radiance and BOA reflectance data cubes were downloaded from the PRISMA mission portal in HDF5 format. A detailed description of the processing is available in the PRISMA Products Specification Document (ASI, PRISMA Products Specification Document, Issue 2.1, accessed on 16 November 2023). All data presented in this study were produced by the latest version of the PRISMA processor (v_4_1_0_02_05).

For Torgnon, PRISMA data were acquired on 15 February 2020 in fairly clear sky with a few cirrus clouds (Figure 4a). The acquisition features the following characteristics: SZA = 61°, View Zenith Angle (VZA) = 8.7°–10.2°, Solar Azimuth Angle (SAA) = 159°, Relative Azimuth Angle (RAA) = 55°. The area covered by the PRISMA image was characterized by a distributed snow cover. Given the timing of the acquisition, most of the snow was in the accumulation period (Colombo et al., 2019), thus fresh and highly reflective. This type of snow is particularly challenging for optical remote sensing (Dozier & Painter, 2004).

For Plateau Rosa, the PRISMA image was acquired on 9 July 2020 in clear sky conditions (Figure 4b). The acquisition features the following characteristics: SZA = 27°, VZA = 8.7°–10.2°, SAA = 145°, RAA = 55°. The area covered by the PRISMA image includes several glaciers during the melting season. In particular, the area of Plateau Rosa was characterized by aged snow (large grain size) and the presence of mineral dust on snow (Di Mauro et al., 2015).

For the Nansen Ice Shelf, the PRISMA scene was acquired on 4th December 2022 in clear sky conditions (Figure 4c). The acquisition features the following characteristics: SZA = 59.3°, VZA = 7.1°, SAA = 59.9°, RAA = 67.5°.

PRISMA imagery were also compared to Sentinel-2 multispectral data due to their large contribution for snow monitoring (Gascoin et al., 2019, 2020). Three Sentinel-2 scenes closer to the PRISMA acquisitions were downloaded from the ESA repository. Torgnon data were acquired on 14th February 2020, the Plateau Rosa scene was acquired on 8th July 2020, and Nansen Ice Shelf data were acquired on 4th December 2022. Sentinel-2 L1 TOA reflectance data were converted to radiance using the SNAP software. For the BOA reflectance comparison, we made use of the Sentinel-2 L2A reflectance product. In Table 1, we summarized information on the three sites used in this study.

23335084, 2024, 7, Downloaded from https://agupubs.onlinelibrary.wiley.com/doi/10.1029/2023EA003482 by CochraneItalia, Wiley Online Library on [16/05/2025]. See the Terms and Conditions (https://onlinelibrary.wiley.com/terms-and-conditions) on Wiley Online Library for rules of use; OA articles are governed by the applicable Creative Commons License

23335084, 2024, 7, Downloaded from https://agupubs.onlinelibrary.wiley.com/doi/10.1029/2023EA003482 by CochraneItalia, Wiley Online Library on [16/05/2025]. See the Terms and Conditions (https://onlinelibrary.wiley.com/terms-and-conditions) on Wiley Online Library for rules of use; OA articles are governed by the applicable Creative Commons License

Table 1
Summary of the Three Sites Used in This Study

Site name	Latitude	Longitude	Elevation	Field campaign date	PRISMA acquisition date	Sentinel-2 acquisition date
Torgnon	45°50′40″N	7°34′41″E	2,160 m	15th February 2020	15th February 2020	14th February 2020
Plateau Rosa	45°56′6″N	7°42′36″E	3,500 m	9th July 2020	9th July 2020	8th July 2020
Nansen Ice Shelf	74°45′20″S	163°27′26″E	75 m	5th December 2022	4th December 2022	4th December 2022

Note. For each site, we reported latitude, longitude, elevation, date of the field campaign, date of PRISMA acquisition and date of Sentinel-2 acquisition.

2.4. Propagation at TOA Radiance

The in situ surface reflectance measurements were propagated to TOA radiance using the MODTRAN5 radiative transfer code (Berk et al., 2011) and compared with satellite observations. The radiative transfer simulations were performed at high resolution by using a band model at 1 cm^{-1} in the 390–2,500 nm spectral range and convolved with nominal values of PRISMA band center wavelengths and FWHM to be compared with L1 TOA radiance spectra. The atmospheric transfer functions used to propagate the surface reflectance to TOA radiance were calculated with MODTRAN5 by means of the Modtran Interrogation Technique. AOT at 550 nm and column water vapor derived from coincident sunphotometer measurements were used as input parameters. The mid-latitude winter/summer atmospheric profiles, the solar irradiance spectrum and rural aerosol models were considered to simulate TOA radiance (Thuillier et al., 2003). The line-of-sight parameters were defined according to the solar zenith and azimuth angles (SZA and SAA) at the time of the PRISMA acquisitions, while the view zenith angle (VZA) was fixed according to the actual PRISMA roll angle in the image center coordinates. DISORT multiple scattering and the correlated-k options were activated to ensure accurate simulations within the atmospheric absorption bands.

2.5. Comparison of Reflectance Products: L2D and Optimal Estimation

PRISMA L2D product consist in the geolocated and geocoded atmospherically corrected BOA reflectance. This product has been downloaded from the PRISMA web portal (https://prisma.asi.it/). In addition to the PRISMA L2D product, we applied an alternative atmospheric correction approach and likewise validated the results with the field observations. The method is based on Optimal Estimation (OE) and was initially introduced for the

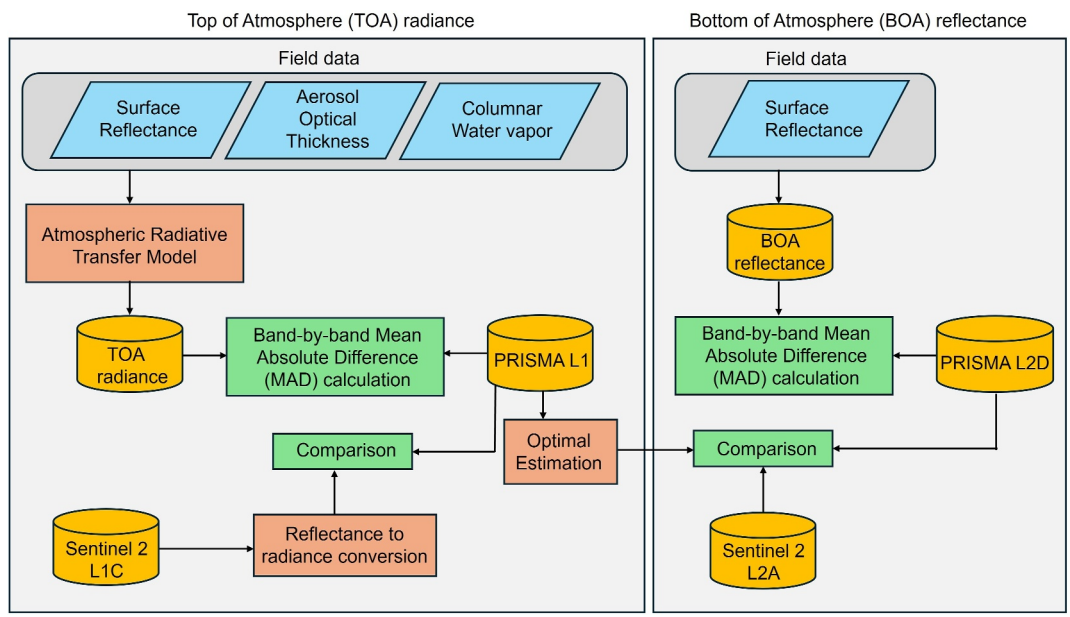

Figure 5. Flowchart showing the match-up analysis used for PRISMA TOA radiance data (left panel) and PRISMA BOA reflectance data (right panel).

23335084, 2024, 7, Downloaded from https://agupubs.onlinelibrary.wiley.com/doi/10.1029/2023EA003482 by CochraneItalia, Wiley Online Library on [16/05/2025]. See the Terms and Conditions (https://onlinelibrary.wiley.com/terms-and-conditions) on Wiley Online Library for rules of use; OA articles are governed by the applicable Creative Commons License

atmospheric correction of hyperspectral images collected by the NASA's AVIRIS-NG airborne instrument (Rodgers, 2000; Thompson et al., 2018). It simultaneously solves for atmosphere and surface state by relying on Bayes' theorem of joint probabilities, and incorporates prior knowledge, measurement noise, as well as model uncertainties in the retrieval framework. The unique coupling of atmosphere and surface properties in the optimized state vector is provided by a combination of the MODTRAN radiative transfer code and a collection of reflectance spectra that serve as prior knowledge. The latter can be obtained either from field measurements or from model simulations. One of the advantages of OE is a comprehensive quantification of posterior uncertainties that are assumed to follow a Gaussian distribution. Recent studies have applied the approach to both synthetic and real measurements from spaceborne imaging spectrometers, including PRISMA and EnMAP, showing promising potential for a global applicability (Bohn et al., 2021, 2022).

2.6. Match-Up Analysis

The comparison between field and satellite data was conducted following Cogliati et al. (2021). A similar approach has also been used for other natural surfaces (Giardino et al., 2020; Pepe et al., 2020; Pignatti et al., 2022; Tagliabue et al., 2022). PRISMA spectra were extracted from the pixels corresponding to the area sampled on the ground and then compared with field spectroscopy data. The same procedure has been conducted on Sentinel-2 imagery, but those data were spatially resampled to 30 m resolution for the comparison with PRISMA. For the evaluation of both TOA and BOA products, the shapes of radiance and reflectance spectra were visually compared across the data set, and the Mean Absolute Difference (MAD) was calculated for each band in order to quantify the agreement between satellite and field spectroscopy data. Regarding the BOA reflectance comparison, the following spectral intervals were excluded because affected by atmospheric water vapor residuals: 900–980 nm; 1,119–1,160 nm; 1,300–1,550 nm; 1,750–2,100 nm. The match-up analysis is presented as a flowchart in Figure 5. Regarding TOA radiance data, we decided to use the L1 PRISMA product in order to evaluate the data product before the atmospheric correction. Conversely, regarding the reflectance BOA data, we chose the L2D PRISMA product (the geocoded version of the at-surface reflectance product) in order to evaluate the product after the atmospheric correction and geocoding. We followed this method also according to previous studies (Giardino et al., 2020; Pellegrino et al., 2023).

3. Results and Discussion

3.1. TOA Radiance Comparisons

The comparisons between satellite TOA (L1 PRISMA and L1 Sentinel-2) and field spectroscopy data (Spectral Evolution, RoX, and ASD Hand-held) are respectively presented in Figure 6 for Torgnon, Figure 7 for Plateau Rosa, and Figure 8 for Nansen Ice Shelf. The visual comparison between different radiance spectra is promising, since we obtained a MAD lower than 5% for most of the spectral range apart from Torgnon, where larger deviation of TOA radiance (MAD > 5% for most wavelengths) were observed. We ascribed this discrepancy to the high cirrus clouds that were present in the sky at the time of measurements and the higher topographic complexity of the site. RoX and Spectral Evolution are closely correlated. Those data were in fact acquired on the same day a few meters apart and this discrepancy may explain the difference to PRISMA data (acquired on 15th February 2020). Conversely, for Plateau Rosa we observed a very good agreement between Spectral Evolution TOA radiance data and the PRISMA L1 product. For this case, also Sentinel-2 L1C data show a good match-up with other data sources. In this site, we obtained the best results of our validation exercise. This could be due to perfect clear sky at the site during the campaign, and to the high elevation and flatness of Plateau Rosa. In fact, those two conditions are arguably the best ones for match-up analyses of satellite hyperspectral data for snow and they represent the best scenario for cal/val sites. For our analysis at the Nansen Ice Shelf, we observed MAD < 5% for the 400–500 nm spectral range and MAD > 5% for larger wavelengths. We observed MAD values of approximately 10% for the 500–900 nm range, and even higher for wavelengths >900 nm. For this campaign, we remark that the field observations and satellite acquisition were collected in two subsequent days, thus this variability can be ascribed to the slightly different atmospheric conditions in the 2 days.

10.1029/2023EA003482

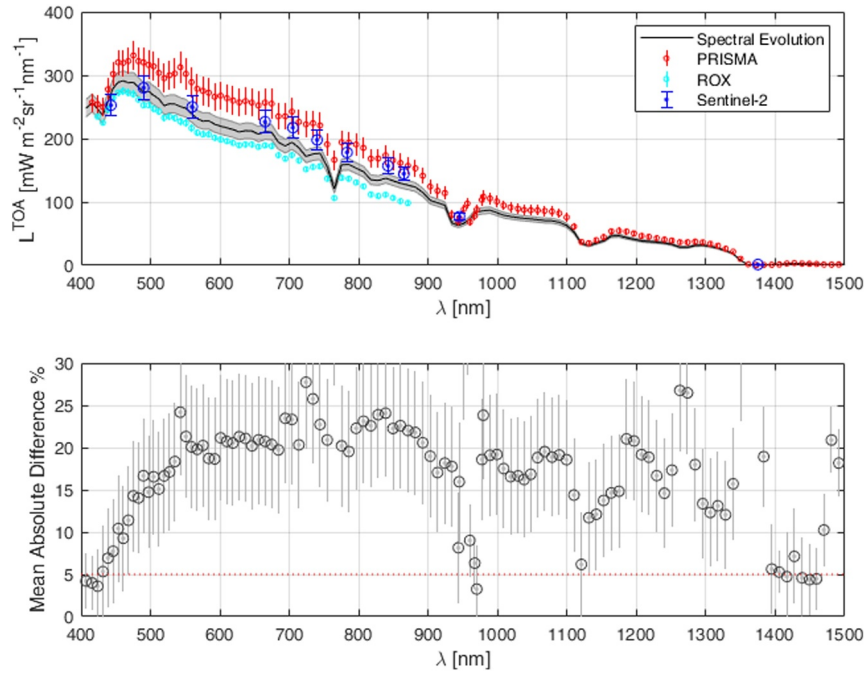

Figure 6. Upper panel: comparison of Top of Atmosphere (TOA) radiance from PRISMA L1 (red points), Spectral Evolution (black line), RoX (cyan line) and Sentinel-2 (blue points) for the Torgnon site. Lower panel: mean absolute difference [%] between PRISMA and Spectral Evolution data. Dotted red line in the lower panel indicates 5% difference threshold in the absolute radiometric accuracy requirement of the PRISMA mission.

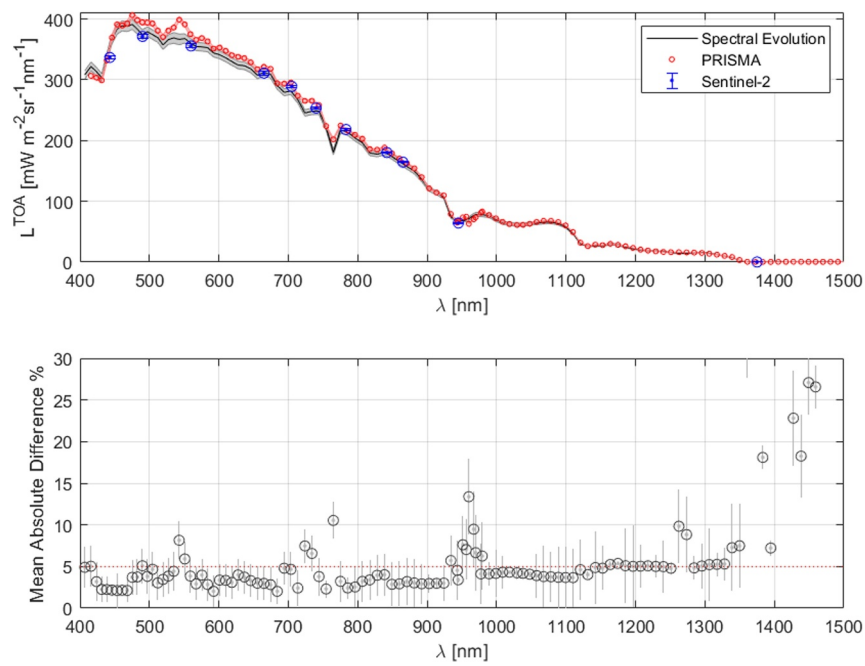

Figure 7. Upper panel: comparison of Top of Atmosphere (TOA) radiance from PRISMA L1 (red points), Spectral Evolution (black line) and Sentinel-2 (blue points) for the Plateau Rosa site. Lower panel: mean absolute difference [%] between PRISMA and Spectral Evolution data. Dotted red line in the lower panel indicates 5% difference threshold in the absolute radiometric accuracy requirement of the PRISMA mission.

23335084, 2024, 7, Downloaded from https://agupubs.onlinelibrary.wiley.com/doi/10.1029/2023EA003482 by CochraneItalia, Wiley Online Library on [16/05/2025]. See the Terms and Conditions (https://onlinelibrary.wiley.com/terms-and-conditions) on Wiley Online Library for rules of use; OA articles are governed by the applicable Creative Commons License

10.1029/2023EA003482

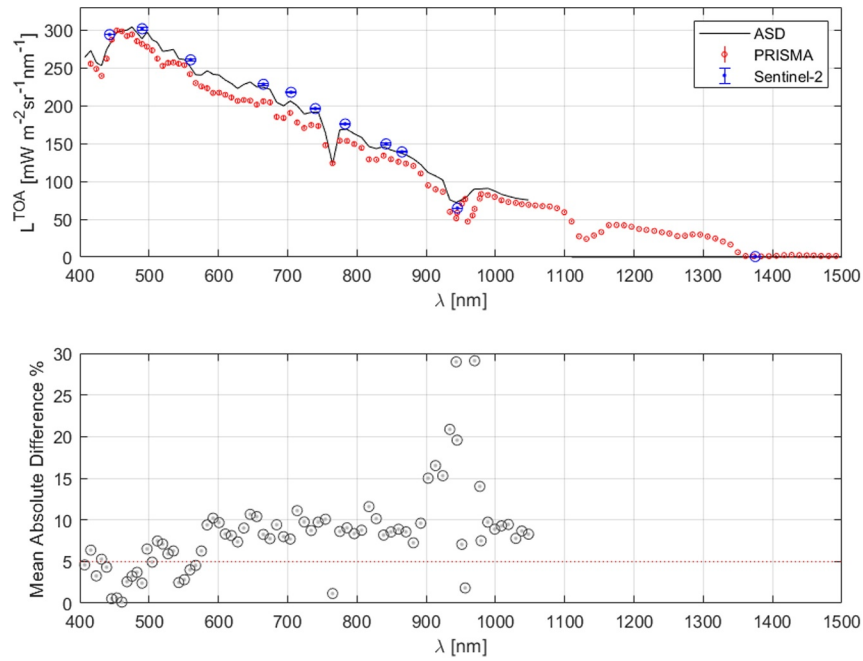

Figure 8. Upper panel: comparison of Top of Atmosphere (TOA) radiance from PRISMA L1 (red points), ASD (black line) and Sentinel-2 (blue points) for the Nansen Ice Shelf site. Lower panel: mean absolute difference [%] between PRISMA and ASD data. Dotted red line in the lower panel indicates 5% difference threshold in the absolute radiometric accuracy requirement of the PRISMA mission.

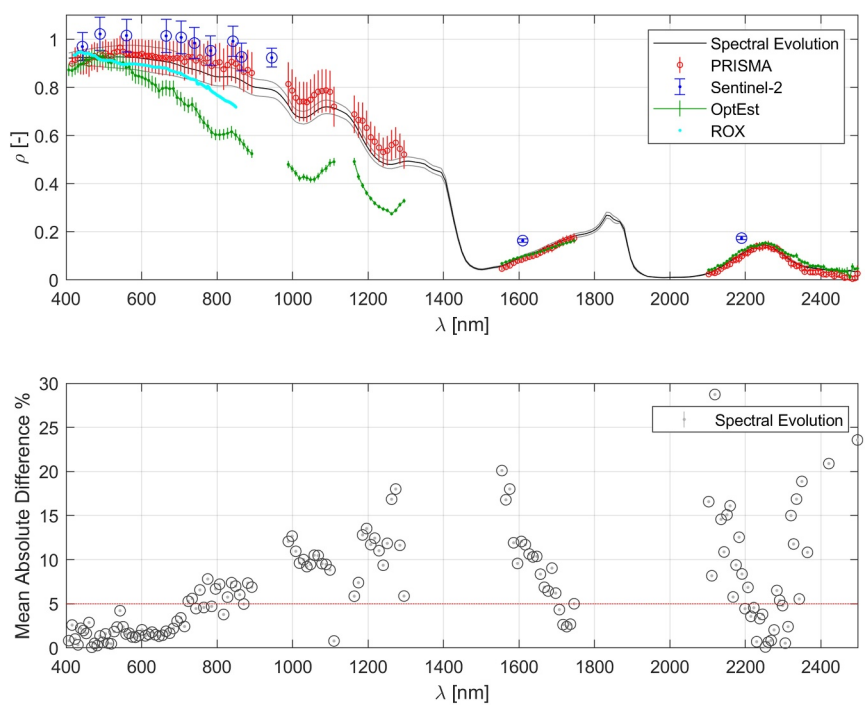

Figure 9. Upper panel: comparison of Bottom of Atmosphere (BOA) reflectance from PRISMA L2D (red points), Optimal Estimation (green points), Spectral Evolution (black line), RoX (cyan line) and Sentinel-2 (blue points) for the Torgnon site. Lower panel: mean absolute difference [%] between Spectral Evolution data and PRISMA L2D. Dotted red line in the lower panel indicates 5% difference threshold in the absolute radiometric accuracy requirement of the PRISMA mission.

23335084, 2024, 7, Downloaded from https://agupubs.onlinelibrary.wiley.com/doi/10.1029/2023EA003482 by CochraneItalia, Wiley Online Library on [16/05/2025]. See the Terms and Conditions (https://onlinelibrary.wiley.com/terms-and-conditions) on Wiley Online Library for rules of use; OA articles are governed by the applicable Creative Commons License

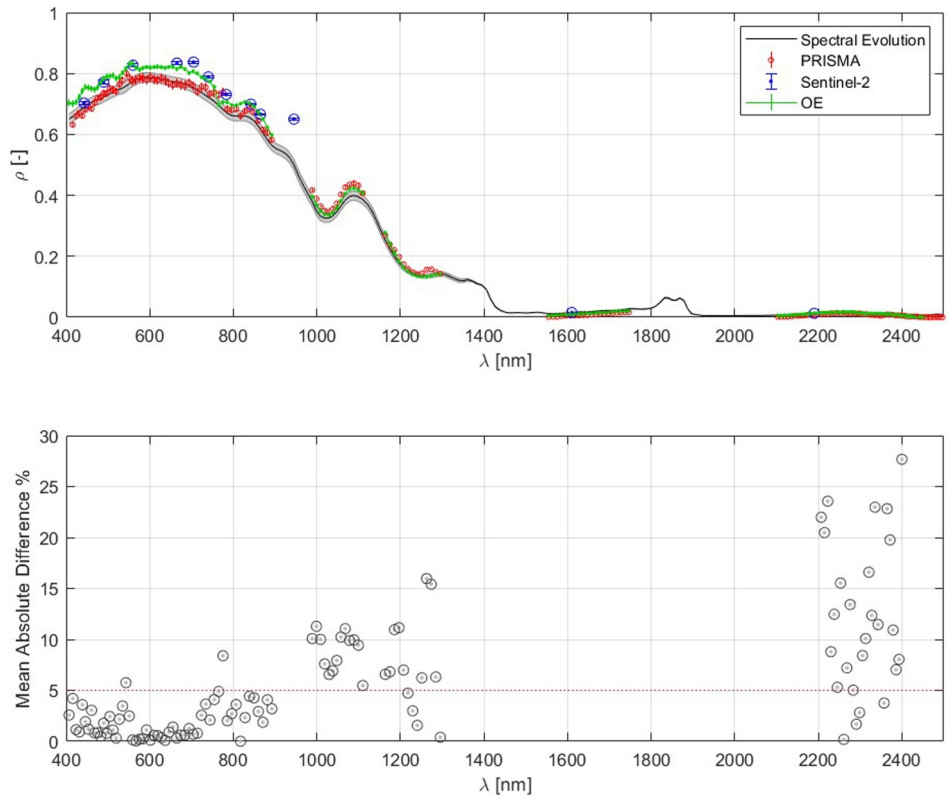

Figure 10. Upper panel: comparison of Bottom of Atmosphere (BOA) reflectance from PRISMA L2D (red points), Optimal Estimation (green points), Spectral Evolution (black line) and Sentinel-2 (blue points) for the Plateau Rosa site. Lower panel: mean absolute difference [%] between Spectral Evolution data and PRISMA L2D (white points). Dotted red line in the lower panel indicates 5% difference threshold in the absolute radiometric accuracy requirement of the PRISMA mission.

3.2. BOA Reflectance Comparisons

The comparisons of BOA data are shown in Figures 9–11 for Torgnon, Pleateau Rosa, and the Nansen Ice Shelf, respectively. As expected, we observed a higher variability in BOA reflectance comparison with respect to TOA radiance. More in detail, for Torgnon we obtained a good agreement between PRISMA L2D and Spectral Evolution data, with a MAD lower than 5% for the spectral range 400–700 nm (Figure 9) while for wavelengths higher than 700 nm the difference was larger than 5%. In particular, some bands in the SWIR showed even higher differences. This is probably due to the metric that we used here for assessing the accuracy of PRISMA observations. In fact, for lower values of reflectance, even slight differences between field and satellite data may result in higher MAD values. RoX spectra showed a good agreement for most of the wavelength range of this instrument (400–850 nm), but we observed that the error in the NIR is higher with respect to the visible wavelengths. Results from the Optimal Estimation approach applied to PRISMA L1 data are in agreement with RoX, Spectral Evolution and PRISMA data in the visible wavelenghts. For longer wavelengths, the spectra showed a marked divergence. We noticed that the PRISMA BOA data obtained with the OE better agree with RoX measurements in the 400–900 nm range compared to the standard L2D PRISMA product. In fact, both the L2 PRISMA product and Spectral Evolution field data show a flat spectrum in the visible wavelenghts, while both Rox and PRISMA OE show a slightly decreasing trend. Sentinel-2 data show higher values in visible and near infrared wavelength range with respect to field and satellite spectra. Overall, Sentinel-2 data show a positive offset equal to 0.03–0.05 reflectance.

Regarding Plateau Rosa, we observed a good match (MAD < 5%) for most of the spectral range of interest between field spectroscopy data and the PRISMA L2D standard product. In this area, snow properties were rather homogeneus. This characteristic is confirmed by the low standard deviations observed in different data sources.

23335084, 2024, 7, Downloaded from https://agupubs.onlinelibrary.wiley.com/doi/10.1029/2023EA003482 by CochraneItalia, Wiley Online Library on [16/05/2025]. See the Terms and Conditions (https://onlinelibrary.wiley.com/terms-and-conditions) on Wiley Online Library for rules of use; OA articles are governed by the applicable Creative Commons License

10.1029/2023EA003482

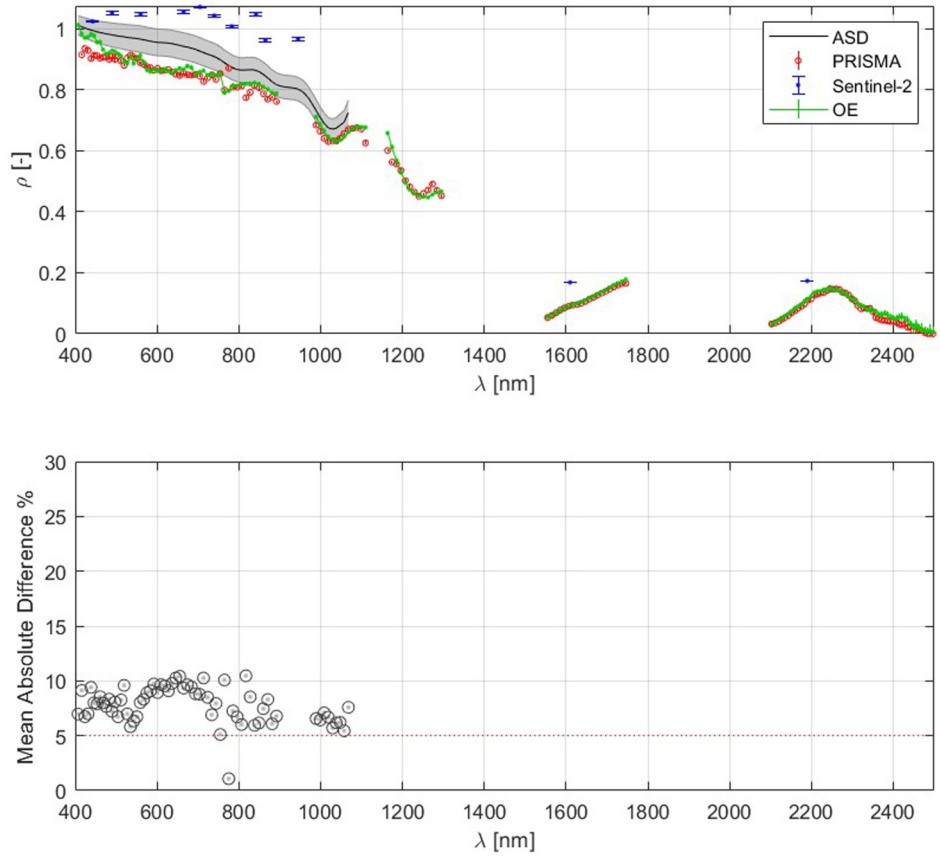

Figure 11. Upper panel: comparison of Bottom of Atmosphere (BOA) reflectance from PRISMA L2D (red points), Optimal Estimation (green points), ASD (black line) and Sentinel-2 (blue points) for the Nansen Ice Shelf site. Lower panel: mean absolute difference [%] between ASD data and PRISMA L2D (white points). Dotted red line in the lower panel indicates 5% difference threshold in the absolute radiometric accuracy requirement of the PRISMA mission.

As described in Section 2.2, the snow surface was covered with a dust layer. This induces a typical bending of the reflectance for wavelenghts lower than 600 nm in all data analyzed in this study. PRISMA L2D, Spectral Evolution, OE, and Sentinel-2 show a similar behavior in the visible range. MAD is lower than 5% in the visible and near infrared wavelength ranges. We observed a divergence (MAD > 5%) between satellite products and field data for wavelengths higher than 1,000 nm. The 1,030 nm absorption feature is particularly well resolved both in PRISMA L2D and OE. This is an encouraging result since features in this spectral region are often employed to retrieve grain size and liquid water content (Donahue et al., 2022; Dozier et al., 2009; Green et al., 2002; Nolin & Dozier, 2000).

Match-up analysis of BOA reflectance from the Nansen Ice Shelf site showed a good agreement in the shape of spectra among different data sources (Figure 10). We measured MAD values between 5% and 10% for all the visible and near infrared bands. In fact, a bias is displayed between ASD and PRISMA L2D data. This again can be ascribed to the 1-day delay between those measurements. As for the OE reflectance data, they resemble the PRISMA L2D standard product for all investigated wavelengths. On the contrary, Sentinel-2 L2 reflectance data showed higher values for all bands.

We should consider that only S2 data provide a normalization for topography. The assumption of lambertian surface is used in all three atmospheric correction schemes. Overall, the results are encouraging and snow covered surface demonstrate their potential to be used as target for vicarious cal/val activities, due to their characteristic optical properties.

23335084, 2024, 7, Downloaded from https://agupubs.onlinelibrary.wiley.com/doi/10.1029/2023EA003482 by CochraneItalia, Wiley Online Library on [16/05/2025]. See the Terms and Conditions (https://onlinelibrary.wiley.com/terms-and-conditions) on Wiley Online Library for rules of use; OA articles are governed by the applicable Creative Commons License

23335084, 2024, 7, Downloaded from https://agupubs.onlinelibrary.wiley.com/doi/10.1029/2023EA003482 by CochraneItalia, Wiley Online Library on [16/05/2025]. See the Terms and Conditions (https://onlinelibrary.wiley.com/terms-and-conditions) on Wiley Online Library for rules of use; OA articles are governed by the applicable Creative Commons License

PRISMA imagery analyzed in this study featured an overall good quality and did not show noisy lines as reported in the recent literature (Amici & Piscini, 2021; Sajadi et al., 2022). This is probably due to a recent improvements (dated 10th October 2022) in the PRISMA processor that was aimed at the removal of across-task black bands in the hyperspectral data (https://prisma.asi.it/missionselect/Latest_news.pdf). All PRISMA data analyzed in this study have been downloaded from the ASI repository after the above described improvements.

3.3. Considerations for Cal/Val Sites

The site of Torgnon features a higher topographic variability compared to Plateau Rosa and the Nansen Ice Shelf. This could explain part of the uncertainties in the match-up analysis. It is well known that changes in slope, aspect, and roughness have a major impact on the optical signal exploited to estimate snow geophysical parameters (Painter & Dozier, 2004; Picard et al., 2020). Furthermore, the Torgnon site is surrounded by snow-covered mountains and this could increase the complexity of cal/val activities because of the contribution of the diffuse radiation and adjacency effects. Those two effects are particularly difficult to correct, and they may also result in BOA reflectance values greater than 1. The Plateau Rosa site is flat and located at high elevation (3,500 m). We note that this site provided the best results in terms of MAD values. Furthermore, aged snow features a lower reflectance compared to fresh snow, which minimizes the possibility of having higher errors between field and satellite data. Results from East Antarctica showed MAD values lower than 10%, as the Nansen Ice Shelf is a very homogenous area. Furthermore, it is easily reachable by helicopter from the italian Mario Zucchelli Station (MZS) located in Baia Terra Nova, which justifies its selection.

In general, future cal/val site for satellite imaging spectroscopy missions should be located in flat areas in polar regions or high altitude alpine sites. Our results showed that PRISMA is able to provide consistent measurements in snow-covered areas. Nevertheless, we highlight the need for a dedicated PRISMA atmospheric and topographic correction algorithm for snow in rugged topography. The single point measurments from automated field spectrometer can however be applied only under specific situations and a protocol for capturing the spatial variability may perform better. During the winter season, snow covered Alpine lakes at high elevation may represents a valuable solution for cal/val activities.

4. Conclusions

In this paper, we presented a first match-up analysis between PRISMA/Sentinel-2 data and contemporary field spectroscopy measurements of snow surface. We built our comparison on two field campaigns conducted in the European Western Alps and in East Antarctica. We found a general good agreement of PRISMA and Sentinel-2 L1 data with propagated TOA radiances from field data. The MAD values were lower than 5% for most of the wavelengths of interest for the retrieval of snow and ice parameters. The highest MAD values were observed for the site of Torgnon, which features a higher topographic complexity and some cirrus clouds during PRISMA acquisition. The comparison of BOA reflectance of PRISMA/Sentinel-2 and field spectroscopy data showed higher variability for wavelengths greater than 800 nm for the Alpine sites. For the Torgnon site, OE strongly diverged from field reflectance in the NIR portion of the spectrum. For Plateau Rosa we obtained the best comparison among different surface reflectance data, with MAD values lower than 5% for the 400–900 nm range. The Nansen Ice Shelf instead showed MAD values <10% between PRISMA L2D and field data, while Sentinel-2 BOA reflectance showed higher values than other data sources.

Our match-up analysis provided encouraging results for the use of PRISMA for snow remote sensing, but also highlighted the need for a dedicated atmospheric and topographic correction algorithm for snow. To this aim, a network of fixed position autonomous hyperspectral radiometers over snow- and ice-covered areas in different regions of the planet is recommendable. In fact, the difficulties in synchronizing field campaigns and PRISMA acquisitions may prevent an accurate analysis of the signal in different snow and atmospheric conditions, while such networks would allow to compile a higher number of match-ups between satellite and field data.

Overall, with the availability of PRISMA scenes over snow- and ice-covered areas of the planet, new opportunities for snow parameter retrievals (e.g., albedo, grain size and shape, liquid water content, concentration and radiative forcing of impurities etc.) were opened. While PRISMA does not acquire images as continuously as other optical satellite missions (i.e., Sentinel-2, Landsat-8 etc.), it allows detailed studies of the cryosphere both at midlatitudes and at the poles.

23335084, 2024, 7, Downloaded from https://agupubs.onlinelibrary.wiley.com/doi/10.1029/2023EA003482 by CochraneItalia, Wiley Online Library on [16/05/2025]. See the Terms and Conditions (https://onlinelibrary.wiley.com/terms-and-conditions) on Wiley Online Library for rules of use; OA articles are governed by the applicable Creative Commons License

Data Availability Statement

PRISMA L1 and L2D products are stored in the open prisma portal (https://prisma.asi.it/). Sentinel-2 data are stored in the Copernicus data space (https://dataspace.copernicus.eu/). Field spectroscopy data, PRISMA data, OE retrieval and MADs values are available at this open repository (Di Mauro, 2024): https://data.mendeley.com/datasets/8pzk3f484z/1.

Acknowledgments
This research was funded by Agenzia Spaziale Italiana (ASI), in the context of PRISCAV project (Attività scientifica di CAL/VAL della missione PRISMA) Grant 2019-5-HH.O. The Antarctic campaign was conducted within the BioGeoAlbedo project (PNRA18_00222), funded by Programma Nazionale di Ricerca in Antartide (PNRA). Genesio L. (CNR-IBE), Matta E. (CNR-IRPI) and Pepe M. (CNR-IREA) are acknowledged for tasking PRISMA acquisitions. RoX data processing was made by using two R packages (FieldSpectrocospyCC and FieldSpectrocospyDP) available at https://github.com/tommasojulitta/. A. Kokhanovsky acknowledges the support of the EnMAP science program under the Space Agency at the DLR with resources from the German Federal Ministry of Economic Affairs and Climate Action (Grant 50EE1923). A portion of this research took place at the Jet Propulsion Laboratory, California Institute of Technology, under a contract with the National Aeronautics and Space Administration (80NM0018D0004). Data/Information generated by Dr. Biagio Di Mauro under an ASI License to Use; Original PRISMA Product—© ASI—(2020, 2022).

References

Amici, S., & Piscini, A. (2021). Exploring PRISMA scene for fire detection: Case study of 2019 bushfires in Ben Halls Gap National Park, NSW, Australia. *Remote Sensing*, *13*(8), 1410. https://doi.org/10.3390/rs13081410

Berk, A., Anderson, G. P., Acharya, P. K., & Shettle, E. P. (2011). MODTRAN® 5.2.1 USER'S MANUAL.

Bohn, N., Di Mauro, B., Colombo, R., Thompson, D. R., Susiluoto, J., Carmon, N., et al. (2022). Glacier ice surface properties in South-West Greenland Ice Sheet: First estimates from PRISMA imaging spectroscopy data. *Journal of Geophysical Research: Biogeosciences*, *127*(3), e2021JG006718. https://doi.org/10.1029/2021JG006718

Bohn, N., Painter, T. H., Thompson, D. R., Carmon, N., Susiluoto, J., Turmon, M. J., et al. (2021). Optimal estimation of snow and ice surface parameters from imaging spectroscopy measurements. *Remote Sensing of Environment*, *264*, 112613. https://doi.org/10.1016/J.RSE.2021.112613

Casey, K. A., & Kääb, A. (2012). Estimation of supraglacial dust and debris geochemical composition via satellite reflectance and emissivity. *Remote Sensing*, *4*(12), 2554–2575. https://doi.org/10.3390/rs4092554

Casey, K. A., Kääb, A., & Benn, D. I. (2012). Geochemical characterization of supraglacial debris via in situ and optical remote sensing methods: A case study in Khumbu Himalaya, Nepal. *The Cryosphere*, *6*(1), 85–100. https://doi.org/10.5194/tc-6-85-2012

Cogliati, S., Rossini, M., Julitta, T., Meroni, M., Schickling, A., Burkart, A., et al. (2015). Continuous and long-term measurements of reflectance and sun-induced chlorophyll fluorescence by using novel automated field spectroscopy systems. *Remote Sensing of Environment*, *164*, 270–281. https://doi.org/10.1016/J.RSE.2015.03.027

Cogliati, S., Sarti, F., Chiarantini, L., Cosi, M., Lorusso, R., Lopinto, E., et al. (2021). The PRISMA imaging spectroscopy mission: Overview and first performance analysis. *Remote Sensing of Environment*, *262*, 112499. https://doi.org/10.1016/J.RSE.2021.112499

Colombo, R., Garzonio, R., Di Mauro, B., Dumont, M., Tuzet, F., Cogliati, S., et al. (2019). Introducing thermal inertia for monitoring snowmelt processes with remote sensing. *Geophysical Research Letters*, *46*(8), 4308–4319. https://doi.org/10.1029/2019GL082193

Di Mauro, B. (2024). Hyperspectral data for PRISMA L1 and L2D validation over snow [Dataset]. *Mendeley Data V1*. https://doi.org/10.17632/8pzk3f484z.1

Di Mauro, B., Baccolo, G., Garzonio, R., Giardino, C., Massabò, D., Piazzalunga, A., et al. (2017). Impact of impurities and cryoconite on the optical properties of the Morteratsch Glacier (Swiss Alps). *The Cryosphere*, *11*(6), 2393–2409. https://doi.org/10.5194/tc-11-2393-2017

Di Mauro, B., Fava, F., Ferrero, L., Garzonio, R., Baccolo, G., Delmonte, B., & Colombo, R. (2015). Mineral dust impact on snow radiative properties in the European Alps combining ground, UAV, and satellite observations. *Journal of Geophysical Research: Atmospheres*, *120*(12), 6080–6097. https://doi.org/10.1002/2015JD023287

Di Mauro, B., Garzonio, R., Rossini, M., Filippa, G., Pogliotti, P., Galvagno, M., et al. (2019). Saharan dust events in the European Alps: Role in snowmelt and geochemical characterization. *The Cryosphere*, *13*(4), 1147–1165. https://doi.org/10.5194/tc-13-1147-2019

Donahue, C., Skiles, S. M., & Hammonds, K. (2022). Mapping liquid water content in snow at the millimeter scale: An intercomparison of mixed-phase optical property models using hyperspectral imaging and in situ measurements. *The Cryosphere*, *16*(1), 43–59. https://doi.org/10.5194/tc-16-43-2022

Dozier, J., Green, R. O., Nolin, A. W., & Painter, T. H. (2009). Interpretation of snow properties from imaging spectrometry. *Remote Sensing of Environment*, *113*, S25–S37. https://doi.org/10.1016/j.rse.2007.07.029

Dozier, J., & Painter, T. H. (2004). Multispectral and hyperspectral remote sensing of Alpine snow properties. *Annual Review of Earth and Planetary Sciences*, *32*(1), 465–494. https://doi.org/10.1146/annurev.earth.32.101802.120404

Dumont, M., Arnaud, L., Picard, G., Libois, Q., Lejeune, Y., Nabat, P., et al. (2017). In situ continuous visible and near-infrared spectroscopy of an alpine snowpack. *The Cryosphere*, *11*(3), 1091–1110. https://doi.org/10.5194/tc-11-1091-2017

Gascoin, S., Dumont, Z. B., Deschamps-Berger, C., Marti, F., Salgues, G., López-Moreno, J. I., et al. (2020). Estimating fractional snow cover in open terrain from Sentinel-2 using the normalized difference snow index. *Remote Sensing*, *12*(18), 2904. https://doi.org/10.3390/RS12182904

Gascoin, S., Grizonnet, M., Bouchet, M., Salgues, G., & Hagolle, O. (2019). Theia Snow collection: High-resolution operational snow cover maps from Sentinel-2 and Landsat-8 data. *Earth System Science Data*, *11*(2), 493–514. https://doi.org/10.5194/essd-11-493-2019

Giardino, C., Bresciani, M., Braga, F., Fabbretto, A., Ghirardi, N., Pepe, M., et al. (2020). First evaluation of PRISMA level 1 data for water applications. *Sensors*, *20*(16), 4553. https://doi.org/10.3390/S20164553

Green, R. O., Dozier, J., Roberts, D., & Painter, T. (2002). Spectral snow-reflectance models for grain-size and liquid-water fraction in melting snow for the solar-reflected spectrum. *Annals of Glaciology*, *34*, 71–73. https://doi.org/10.3189/172756402781817987

Green, R. O., Mahowald, N., Ung, C., Thompson, D. R., Bator, L., Bennet, M., et al. (2020). The Earth surface mineral dust source investigation: An Earth science imaging spectroscopy mission. *IEEE Aerospace Conference Proceedings*. https://doi.org/10.1109/AERO47225.2020.9172731

Green, R. O., Painter, T. H., Roberts, D. A., & Dozier, J. (2006). Measuring the expressed abundance of the three phases of water with an imaging spectrometer over melting snow. *Water Resources Research*, *42*(10). https://doi.org/10.1029/2005WR004509

Kokhanovsky, A. (2021). *Snow optics*. Snow Optics. https://doi.org/10.1007/978-3-030-86589-4

Kokhanovsky, A., Di Mauro, B., & Colombo, R. (2022). Snow surface properties derived from PRISMA satellite data over the Nansen Ice Shelf (East Antarctica). *Frontiers in Environmental Science*, *0*, 1420. https://doi.org/10.3389/FENVS.2022.904585

Kokhanovsky, A., Di Mauro, B., Garzonio, R., & Colombo, R. (2021). Retrieval of dust properties from spectral snow reflectance measurements. *Frontiers in Environmental Science*, *9*, 42. https://doi.org/10.3389/fenvs.2021.644551

Kokhanovsky, A., Lamare, M., Danne, O., Brockmann, C., Dumont, M., Picard, G., et al. (2019). Retrieval of snow properties from the Sentinel-3 ocean and land colour instrument. *Remote Sensing*, *11*(19), 2280. https://doi.org/10.3390/rs11192280

Lee, C. M., Glenn, N. F., Stavros, E. N., Luvall, J., Yuen, K., Hain, C., & Schollaert Uz, S. (2022). Systematic integration of applications into the surface biology and geology (SBG) Earth mission architecture study. *Journal of Geophysical Research: Biogeosciences*, *127*(4), e2021JG006720. https://doi.org/10.1029/2021JG006720

Naethe, P., De Sanctis, A., Burkart, A., Campbell, P. K. E., Colombo, R., Di Mauro, B., et al. (2024). Towards a standardized, ground-based network of hyperspectral measurements: Combining time series from autonomous field spectrometers with Sentinel-2. *Remote Sensing of Environment*, *303*, 114013. https://doi.org/10.1016/j.rse.2024.114013

Negi, H. S., & Kokhanovsky, A. (2011). Retrieval of snow grain size and albedo of western Himalayan snow cover using satellite data. *The Cryosphere*, *5*(4), 831–847. https://doi.org/10.5194/tc-5-831-2011

Nieke, J., & Rast, M. (2018). Towards the copernicus hyperspectral imaging mission for the environment (CHIME). In *International Geoscience and Remote Sensing Symposium (IGARSS)* (pp. 157–159). https://doi.org/10.1109/IGARSS.2018.8518384

Nolin, A. W., & Dozier, J. (2000). A hyperspectral method for remotely sensing the grain size of snow. *Remote Sensing of Environment*, *74*(2), 207–216. https://doi.org/10.1016/S0034-4257(00)00111-5

Painter, T. H., & Dozier, J. (2004). Measurements of the hemispherical-directional reflectance of snow at fine spectral and angular resolution. *Journal of Geophysical Research*, *109*(D18). https://doi.org/10.1029/2003JD004458

Painter, T. H., Seidel, F. C., Bryant, A. C., McKenzie Skiles, S., & Rittger, K. (2013). Imaging spectroscopy of albedo and radiative forcing by light-absorbing impurities in mountain snow. *Journal of Geophysical Research: Atmospheres*, *118*(17), 9511–9523. https://doi.org/10.1002/jgrd.50520

Paul, F., Rastner, P., Azzoni, R. S., Diolaiuti, G., Fugazza, D., Bris, R. L., et al. (2020). Glacier shrinkage in the Alps continues unabated as revealed by a new glacier inventory from Sentinel-2. *Earth System Science Data*, *12*(3), 1805–1821. https://doi.org/10.5194/ESSD-12-1805-2020

Pellegrino, A., Fabbretto, A., Bresciani, M., de Lima, T. M. A., Braga, F., Pahlevan, N., et al. (2023). Assessing the accuracy of PRISMA standard reflectance products in globally distributed aquatic sites. *Remote Sensing*, *15*(8), 2163. https://doi.org/10.3390/rs15082163

Pepe, M., Pompilio, L., Gioli, B., Busetto, L., & Boschetti, M. (2020). Detection and classification of non-photosynthetic vegetation from PRISMA hyperspectral data in croplands. *Remote Sensing*, *12*(23), 3903. https://doi.org/10.3390/RS12233903

Picard, G., Dumont, M., Lamare, M., Tuzet, F., Larue, F., Pirazzini, R., & Arnaud, L. (2020). Spectral albedo measurements over snow-covered slopes: Theory and slope effect corrections. *The Cryosphere*, *14*(5), 1497–1517. https://doi.org/10.5194/tc-14-1497-2020

Picard, G., Libois, Q., Arnaud, L., Verin, G., & Dumont, M. (2016). Development and calibration of an automatic spectral albedometer to estimate near-surface snow SSA time series. *The Cryosphere*, *10*(3), 1297–1316. https://doi.org/10.5194/tc-10-1297-2016

Pignatti, S., Amodeo, A., Carfora, M. F., Casa, R., Mona, L., Palombo, A., et al. (2022). PRISMA L1 and L2 Performances within the PRISCAV Project: The Pignola Test Site in Southern Italy. *Remote Sensing*, *14*(9), 1985. https://doi.org/10.3390/RS14091985

Rodgers, C. D. (2000). Inverse methods for atmospheric sounding: Theory and Practice, series on atmospheric, oceanic and planetary physics–Vol. 2. Series on Atmospheric, Oceanic and Planetary Physics, 2.

Sajadi, P., Gholamnia, M., Bonafoni, S., & Pilla, F. (2022). Spectral-based regression model for destriping of abnormal pixel values in PRISMA hyperspectral image. *European Journal of Remote Sensing*, *55*(1), 622–643. https://doi.org/10.1080/22797254.2022.2141659

Salzano, R., Lanconelli, C., Esposito, G., Giusto, M., Montagnoli, M., & Salvatori, R. (2021). On the seasonality of the snow optical behaviour at Ny Ålesund (Svalbard Islands, Norway). *Geosciences*, *11*(3), 112. https://doi.org/10.3390/GEOSCIENCES11030112

Storch, T., Honold, H.-P., Chabrillat, S., Habermeyer, M., Tucker, P., Brell, M., et al. (2023). The EnMAP imaging spectroscopy mission towards operations. *Remote Sensing of Environment*, *294*, 113632. https://doi.org/10.1016/j.rse.2023.113632

Tagliabue, G., Boschetti, M., Bramati, G., Candiani, G., Colombo, R., Nutini, F., et al. (2022). Hybrid retrieval of crop traits from multi-temporal PRISMA hyperspectral imagery. *ISPRS Journal of Photogrammetry and Remote Sensing*, *187*, 362–377. https://doi.org/10.1016/J.ISPRSJPRS.2022.03.014

Thompson, D. R., Green, R. O., Bradley, C., Brodrick, P. G., Mahowald, N., Dor, E. B., et al. (2024). On-orbit calibration and performance of the EMIT imaging spectrometer. *Remote Sensing of Environment*, *303*, 113986. https://doi.org/10.1016/j.rse.2023.113986

Thompson, D. R., Natraj, V., Green, R. O., Helmlinger, M. C., Gao, B. C., & Eastwood, M. L. (2018). Optimal estimation for imaging spectrometer atmospheric correction. *Remote Sensing of Environment*, *216*, 355–373. https://doi.org/10.1016/j.rse.2018.07.003

Thuillier, G., Hersé, M., Labs, D., Foujols, T., Peetermans, W., Gillotay, D., et al. (2003). The solar spectral irradiance from 200 to 2400 nm as measured by the SOLSPEC spectrometer from the Atlas and Eureca Missions. *Solar Physics*, *214*(1), 1–22. https://doi.org/10.1023/A:1024048429145

Warren, S. G. (2019). Optical properties of ice and snow. *Philosophical Transactions of the Royal Society A*, *377*(2146), 20180161. https://doi.org/10.1098/RSTA.2018.0161

Zibordi, G., Meloni, G. P., & Frezzotti, M. (1996). Snow and ice reflectance spectra of the Nansen Ice Sheet surfaces. *Cold Regions Science and Technology*, *24*(2), 147–151. https://doi.org/10.1016/0165-232X(95)00018-7

23335084, 2024, 7, Downloaded from https://agupubs.onlinelibrary.wiley.com/doi/10.1029/2023EA003482 by CochraneItalia, Wiley Online Library on [16/05/2025]. See the Terms and Conditions (https://onlinelibrary.wiley.com/terms-and-conditions) on Wiley Online Library for rules of use; OA articles are governed by the applicable Creative Commons License